RESEARCH/REVIEW ARTICLE

Evaluation of simulated sea-ice concentrations from sea-ice/ocean models using satellite data and polynya classification methods

Susanne Adams,[1] Sascha Willmes,[1] Günther Heinemann,[1] Polona Rozman,[2] Ralph Timmermann[2] & David Schröder[1,3]

[1] Department of Environmental Meteorology, University of Trier, Behringstr. 21, DE-54286 Trier, Germany
[2] Alfred Wegener Institute for Polar and Marine Research, Bussestr. 24, DE-27570 Bremerhaven, Germany
[3] Centre for Polar Observation and Modelling, University College London, Gower Street, WC1E 6BT London, UK

Keywords
Polynyas; sea ice; sea-ice/ocean models; remote sensing.

Correspondence
Susanne Adams, Department of Environmental Meteorology, University of Trier, Behringstr. 21, DE-54286 Trier, Germany.
E-mail: susanne.adams@uni-trier.de

Abstract

Sea-ice concentrations in the Laptev Sea simulated by the coupled North Atlantic–Arctic Ocean–Sea-Ice Model and Finite Element Sea-Ice Ocean Model are evaluated using sea-ice concentrations from Advanced Microwave Scanning Radiometer–Earth Observing System satellite data and a polynya classification method for winter 2007/08. While developed to simulate large-scale sea-ice conditions, both models are analysed here in terms of polynya simulation. The main modification of both models in this study is the implementation of a landfast-ice mask. Simulated sea-ice fields from different model runs are compared with emphasis placed on the impact of this prescribed landfast-ice mask. We demonstrate that sea-ice models are not able to simulate flaw polynyas realistically when used without fast-ice description. Our investigations indicate that without landfast ice and with coarse horizontal resolution the models overestimate the fraction of open water in the polynya. This is not because a realistic polynya appears but due to a larger-scale reduction of ice concentrations and smoothed ice-concentration fields. After implementation of a landfast-ice mask, the polynya location is realistically simulated but the total open-water area is still overestimated in most cases. The study shows that the fast-ice parameterization is essential for model improvements. However, further improvements are necessary in order to progress from the simulation of large-scale features in the Arctic towards a more detailed simulation of smaller-scaled features (here polynyas) in an Arctic shelf sea.

Coupled sea-ice/ocean models are used to simulate the large-scale sea-ice conditions and ocean processes in the Arctic. Primarily, the models were formulated for the realistic simulation of the large-scale features of the Arctic ice–ocean system (Wang et al. 2003; Johnson et al. 2007; Martin & Gerdes 2007). The simulation of smaller-scale features like polynyas is not the main focus of these models. However, polynyas have a great impact on properties such as sea-ice concentration, ice growth and ice thickness as well as water-mass modification and atmospheric circulation patterns (Morales Maqueda et al. 2004; Ebner et al. 2011 [this volume]). The polynyas in the Laptev Sea (Fig. 1) are areas of particular interest, since a considerable fraction of the sea-ice production on Arctic shelf areas is estimated to take place in these polynyas (Dethleff et al. 1998). The realistic simulation of polynya events is a great challenge for current sea-ice/ocean models. An accurate simulation of the polynya

Polar Research 2011. © 2011 S. Adams et al. This is an open-access article distributed under the terms of the Creative Commons Attribution-Noncommercial 3.0 Unported License (http://creativecommons.org/licenses/by-nc/3.0/), permitting all non-commercial use, distribution, and reproduction in any medium, provided the original work is properly cited.
Citation: *Polar Research* 2011, *30*, 7124, DOI: 10.3402/polar.v30i0.7124

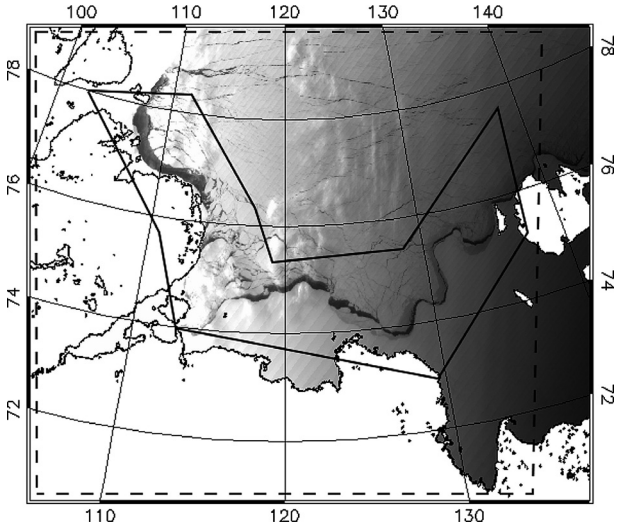

Fig. 1 Moderate Resolution Imaging Spectroradiometer channel 1 image of the Laptev Sea for 22 April 2008, 1055 UTC. The area enclosed by a black solid line denotes the Laptev Sea polynya mask (LAP). The polynyas can be seen as a dark narrow band along the landfast-ice edge (see Fig. 2). The black-dashed rectangle borders the core model domain of the two Finite Element Sea-Ice Ocean Model versions, FESOM-HR and FESOM-FI.

position, as well as shape and size, is needed for a realistic calculation of ice production in coupled sea-ice/ocean models. The evaluation of simulated sea-ice concentrations using satellite data is therefore an important step for quantifying the strengths and the weaknesses of the models.

For the evaluation we use sea-ice concentrations calculated by the Arctic Radiation and Turbulence Interaction Study Sea-Ice (ASI) algorithm from Advanced Microwave Scanning Radiometer–Earth Observing System (AMSR-E) brightness temperatures (Kaleschke et al. 2001; Spreen et al. 2008). In addition, the Polynya Signature Simulation Method (PSSM) is applied to classify thick ice, thin ice and open water from microwave brightness temperatures (Markus & Burns 1995; Kern et al. 2007). The PSSM was used in previous studies to calculate the polynya area from combined open-water and thin-ice areas to investigate polynya dynamics in Arctic and Antarctic polynyas (Renfrew et al. 2002; Kern 2008; Kern 2009).

In this study we evaluate sea-ice concentrations simulated by the coupled North Atlantic–Arctic Ocean–Sea-Ice Model (NAOSIM) and the coupled Finite Element Sea-Ice Ocean Model (FESOM) in the Laptev Sea for the winter season 2007/08 with AMSR-E sea-ice concentrations and PSSM polynya area. We use sea-ice fields from five model runs with different parameterizations to analyse model improvements.

Data sets and techniques

NAOSIM

A data set of simulated sea-ice concentrations is derived from a coupled sea-ice/ocean model of the NAOSIM hierarchy developed at the Alfred Wegener Institute for Polar and Marine Research (Gerdes et al. 2003; Karcher et al. 2003; Fieg et al. 2010). The ocean component of NAOSIM is based on the Geophysical Fluid Dynamics Laboratory Modular Ocean Model (Pacanowski 1995). The sea-ice component is a dynamic-thermodynamic sea-ice model with the thermodynamics following Parkinson & Washington (1979) and a viscous-plastic rheology according to Hibler (1979). The models are coupled in accordance with Hibler & Bryan (1987). The model covers the subpolar North Atlantic, the Nordic seas and the Arctic Ocean. The rotated spherical grid has a spatial resolution of 1/12° (approximately 9 km). The time step is 300 s. The model is forced with daily atmospheric reanalysis fields provided by the US National Centers for Environmental Prediction (NCEP) and the US National Center for Atmospheric Research (Kanamitsu et al. 2002). Surface fluxes of fresh water contain the effects of precipitation (NCEP data), evaporation (bulk formula) and the exchange between ocean and sea ice due to freezing and melting. The difference between ocean and ice velocities enters into the calculation of the ocean sea-ice drag parameterization.

FESOM

For simulating sea-ice concentrations, we also use FESOM's sea-ice component (Timmermann et al. 2009). While the model thermodynamics are very similar to those of NAOSIM, FESOM uses an elastic–viscous–plastic rheology (Hunke & Dukowicz 1997) in the sea-ice momentum balance. To reduce computer costs, our FESOM simulations neglect the horizontal advection (and diffusion) of ocean temperature and salinity. The ocean model is reduced to the computation of turbulent vertical fluxes of heat and salt as a function of the Richardson number. Surface stresses between ice and ocean/atmosphere are quadratic functions of the wind speed and the velocity difference, respectively. Ocean surface currents and vertical shear required as boundary conditions for sea-ice momentum balance and the ocean vertical mixing scheme have been derived from an annual mean of a fully coupled model run.

We use this model in two different configurations: simulations covering the whole of the Arctic are performed on a rotated 1/4° (approximately 25 km) grid (Rollenhagen et al. 2009). Starting from a climatological

Citation: *Polar Research* 2011, *30*, 7124, DOI: 10.3402/polar.v30i0.7124

sea-ice distribution, the model is run over several decades forced with a combination of daily NCEP reanalysis data for 2-m air temperature and 10-m wind, monthly mean humidity from European Centre for Medium-Range Weather Forecasts reanalysis and climatological fields for precipitation and cloud cover. The time step is two hours. A second series of simulations is performed with a regional, high-resolution (1/20°, approximately 5 km) configuration that covers only the Laptev Sea (see Fig. 1). Starting from an initial sea-ice distribution derived from AMSR-E sea-ice concentrations (daily mean of 1 April 2008) and an initial ice thickness of 1 m with a snow layer of 5 cm, we force the model with data from the German Weather Service's Global Model Extended (GME) (Majewski et al. 2002) to specifically simulate the polynya development in April–May 2008. The time step in this version is one hour. A horizontal ice volume diffusivity of 2000 m^2/s in the coarse-scale and 100 m^2/s in the high-resolution configuration is applied.

Retrieval of landfast-ice extent and area

Landfast ice is defined as sea ice that is attached to a shore and does not move with ocean currents or winds. Arctic shelves are covered by landfast ice during a large part of the year. In the Laptev Sea landfast ice shows seasonal variability. It begins to form along the coast in October and reaches its maximum extent in April. The position of the landfast-ice edge then coincides roughly with the position of the 25-m isobaths (see Fig. 2). The break-up of the landfast ice starts at the end of May (Bareiss 2003; Bareiss & Görgen 2005).

Currently sea-ice models are not able to simulate the formation of landfast ice (Wang et al. 2003; König Beatty & Holland 2009). Bathymetry and coastline geometry have already been integrated in sea-ice models but the shear coefficients typically used are too small for the landfast ice to remain fixed to the coast during offshore wind conditions (König Beatty & Holland 2009). The Laptev Sea flaw polynya in the simulations is therefore not produced along the landfast-ice edge but shifted towards the coast. The dislocation of the polynya entails a bias in sea-ice concentration, ice growth, ice thickness and ocean winter temperature and salinity distribution (Wang et al. 2003; Rozman 2009).

To overcome these deficiencies, König Beatty & Holland (2009) developed a simple landfast-sea-ice model by adding the tensile strength to commonly used

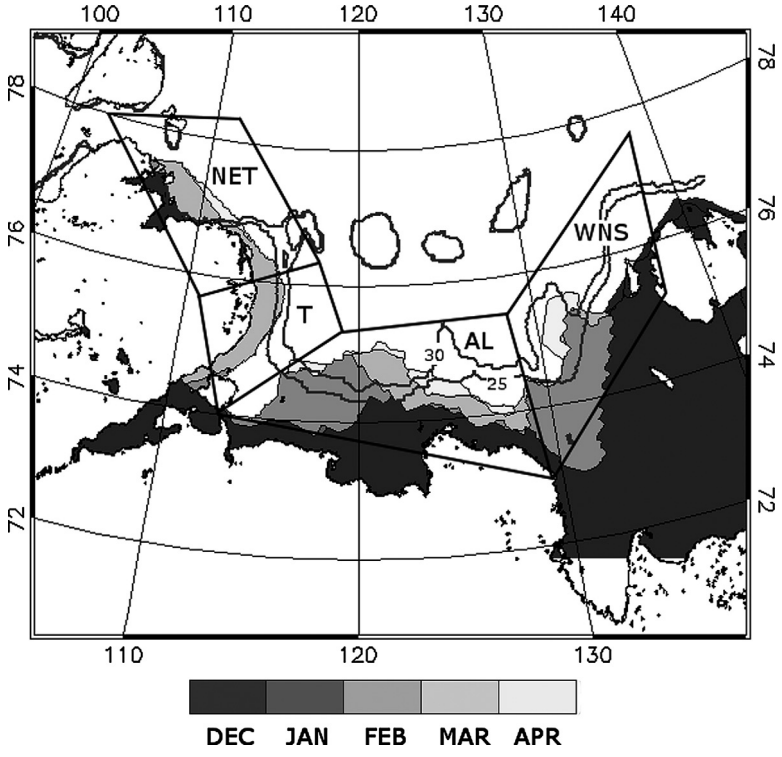

Fig. 2 Landfast-ice masks derived from Moderate Resolution Imaging Spectroradiometer surface temperatures for December 2007 to April 2008. Contour lines show 25- and 30-m isobaths. Black-bordered areas show the different Laptev Sea polynya subsets: the north-eastern Taimyr polynya (NET), the Taimyr polynya (T), the Anabar–Lena polynya (AL) and the western New Siberian polynya (WNS).

viscous–plastic and elastic–viscous–plastic sea-ice rheologies. The model runs with the modified rheologies are able to simulate landfast-ice features. However, the landfast ice breaks up very near to the coast. In reality, the landfast-ice edge is much farther away from the coast. Initial work to add tensile strength to rheology in a finite element model was presented by Lietaer et al. (2008) but failed to simulate landfast-ice structures. Further studies are necessary with the optimum rheology setup integrated in coupled sea-ice/ocean models (König Beatty & Holland 2009).

The mentioned studies show that current sea-ice models are lacking in simulating dynamically landfast ice. Thus, landfast ice has to be prescribed to simulate landfast-ice structures. Lieser (2004) produced a landfast-ice prescription based on bathymetry. All sea ice in coastal regions having a water depth of less than 30 m (see Fig. 2) is classified as immobile landfast ice if the mean ice thickness exceeds 1/10th of the water depth. In terms of model numerics, the respective grid cell is omitted from the grid drift calculations. In summer months landfast ice is reconverted to drift ice to prevent unrealistic ice accumulation in the coastal regions. This simple approach was shown to work well when compared with observations along the Siberian coast (Lieser 2004).

Using a relation between bathymetry and ice thickness as an indicator for landfast ice is only sufficient for models with a coarse spatial resolution as described in Lieser (2004). In general, the landfast-ice edge follows the 20- to 30-m isobath depending on time and region (Barber & Hanesiak 2004; Bareiss & Görgen 2005; Mahoney et al. 2007). However, in some regions the landfast-ice edge can also extend over much deeper water, for example, between the islands of the Canadian Arctic Archipelago and on the Russian continental shelves (König Beatty 2007; Mahoney et al. 2007). The results of these studies show that the use of bathymetry for defining the landfast-ice edge is only a simplification. Landfast ice generally forms in shallow water but there are also many exceptions (see Fig. 2). Hence, the bathymetry is not sufficient to describe accurately the extent of landfast ice in any study that uses a model with a much more detailed spatial resolution and aims at a faithful-in-time reproduction of local processes.

For a realistic coverage of seasonal variability and the extent of the landfast ice, we extract the landfast-ice edge position from available high-resolution observed data (Wang et al. 2003). A monthly landfast-ice mask is derived from December 2007 to April 2008 using high-resolution ($1 \times 1\,km^2$) surface temperatures from the Moderate Resolution Imaging Spectroradiometer (MODIS) sensor. A split-window method is used to calculate the surface temperatures from MODIS infrared channels (Key et al. 1997). For each of the five months, a suitable MODIS scene (cloud-free above the region of the landfast-ice edge) is sought. We utilize the temperature differences between the thicker and colder landfast ice and the thinner and warmer drifting ice. A dynamic ice surface temperature threshold separating landfast ice from drifting ice is defined for each selected MODIS scene. Figure 2 shows the temporal variability of the landfast ice in the Laptev Sea from December to April. As with Lieser (2004), we set drift velocities within the landfast-ice area to zero and the sea-ice momentum balance remains unresolved (Rozman 2009). In June the landfast ice is allowed to drift (Bareiss 2003; Bareiss & Görgen 2005).

Sea-ice concentrations from model data

In this study we use five different sea-ice concentration model data sets obtained from the two sea-ice/ocean models in the Laptev Sea for the 2007/08 winter season (Table 1). The first sea-ice concentration data set is obtained from NAOSIM with the described model settings and the second one from NAOSIM with the same configurations but with an additional prescribed landfast-ice mask. The second model version is abbreviated as NAOSIM-FI in the following sections.

We also use three sea-ice concentration data sets obtained from FESOM. One comes from the model configuration with coarse spatial resolution (FESOM-CR) described by Rollenhagen et al. (2009), the second ice concentration data set is derived from the newly configured fine-scale FESOM model version on a regional grid (FESOM-HR) and the third ice concentration data set is derived from the fine-scale FESOM model version that includes additionally a landfast-ice parameterization. We refer to this model as FESOM-FI.

All model data sets are available as daily averages. The NAOSIM, NAOSIM-FI and FESOM-CR sea-ice concentrations are available for the period 1 November 2007 to 11 May 2008. The FESOM-HR and FESOM-FI ice concentrations are available only for 1 April to 11 May 2008. All model results are interpolated to a common grid of $6.25 \times 6.25\,km^2$, this being the resolution of the AMSR-E evaluation data (see below).

Remote-sensing products

Daily averaged AMSR-E sea-ice concentrations with a spatial resolution of $6.25 \times 6.25\,km^2$ are obtained

Citation: *Polar Research* 2011, *30*, 7124, DOI: 10.3402/polar.v30i0.7124

Table 1 Specifications of the data sets used in this study: two versions of the North Atlantic–Arctic Ocean–Sea-Ice Model (NAOSIM and NAOSIM-FI); three versions of the Finite Element Sea-Ice Ocean Model (FESOM, FESOM-CR and FESOM-FI); the Advanced Microwave Scanning Radiometer–Earth Observing System (AMSR-E) satellite data and the Polynya Signature Simulation Method (PSSM) data.

		NAOSIM		FESOM			AMSR-E	PSSM
		Without landfast ice (NAOSIM)	With landfast ice (NAOSIM-FI)	Without landfast ice, coarse resolution (FESOM-CR)	Without landfast ice, high resolution (FESOM-HR)	With landfast ice, high resolution (FESOM-FI)		
Spatial resolution		1/12°	1/12°	1/4°	1/20°	1/20°	6.25×6.25 km^2	6.25×6.25 km^2
Temporal resolution		Daily mean	Daily mean	Daily mean	Daily mean	Daily mean	Daily mean	Daily mean
Period		1 Nov 2007–11 May 2008	1 Nov 2007–11 May 2008	1 Nov 2007–11 May 2008	1 April 2008–11 May 2008	1 April 2008–11 May 2008	1 Nov 2007–11 May 2008	1 Nov 2007–11 May 2008
Forcing data	Name	NCEP[a]	NCEP	NCEP	GME[b]	GME		
	Spatial res.	1.875°	1.875°	1.875°	0.5°	0.5°		
	Temp. res.	Daily	Daily	Daily	6 hourly	6 hourly		

[a]US National Centers for Environmental Prediction.
[b]Global Model Extended.

for winter 2007/08 from the University of Hamburg (Kaleschke et al. 2001; Spreen et al. 2008).

The PSSM was developed by Markus & Burns (1995). This method iteratively classifies open water, thin ice (a combination of the two determines the polynya area) and thick ice. In our study, it is applied to daily averaged AMSR-E brightness temperatures. The AMSR-E/Aqua Daily L3 brightness temperatures are provided by the US National Snow and Ice Data Center (Cavalieri et al. 2004). The method is based on polarization ratios obtained from AMSR-E brightness temperatures at 36 GHz and 89 GHz. The 89 GHz channel with its finer spatial resolution (6.25×6.25 km^2), but higher atmospheric disturbance, is combined with the 36 GHz channel with the lower spatial resolution (12.5×12.5 km^2) but less weather influence (Kern et al. 2007; Kern 2009). A case study of a polynya event in the Laptev Sea shows that PSSM polynya class includes open water and thin ice up to 0.2 m (Willmes et al. 2010).

Evaluation variables

We divide the Laptev Sea into different polynya areas according to Bareiss & Görgen (2005) (Fig. 2). From north-west to south-east they are the north-eastern Taimyr polynya (NET), the Taimyr polynya (T), the Anabar–Lena polynya (AL) and the western New Siberian polynya (WNS). The WNS and AL polynyas represent the eastern Laptev Sea, T and NET represent the western Laptev Sea. We also use a polynya mask as the sum of all other regions of interest (LAP).

We calculate the open-water area as follows: for each pixel in the region of interest the fraction of open water is determined, multiplied by the pixel area (6.25×6.25 km^2) and summarized for the entire subset:

$$\begin{aligned}\text{open-water area } (m^2) &= \sum_{i=1}^{n}(100 - \text{sea-ice concentration } [\%]) \\ &\quad \times \text{pixel area } (m^2). \end{aligned} \quad (1)$$

Another evaluation variable is the polynya area as calculated by means of an ice-concentration threshold. Since areas with thin ice up to 0.2 m are most important for new ice formation due to the high heat exchange between ocean and atmosphere (Willmes et al. 2011 [this volume]), a comparison with PSSM polynya area (to determine polynyas up to an ice thickness of 0.2 m [Willmes et al. 2010]) and high-resolution MODIS surface temperatures shows that the empirical threshold of 70% sea-ice concentration yields realistic polynya borders (Massom et al. 1998):

$$\text{polynya area } (m^2) = \sum_{i=1}^{n} \text{pixel with sea-ice concentration} < 70\% \times \text{pixel area } (m^2). \quad (2)$$

We distinguish between the two variables, namely, open-water area and polynya area because they yield information about different polynya features. The open-water area shows the mean conditions of the sea-ice concentration in the polynya subsets. The polynya area yields information about the location and the size of the polynya.

Results

Open-water area

Figure 3 shows the time series of open-water area calculated from AMSR-E sea-ice concentrations and from the simulated ice concentrations in the several polynya subsets from November 2007 to May 2008. In most cases the overestimation of the open-water area calculated from the simulated sea-ice concentrations is striking.

The open-water area determined from sea-ice concentrations of NAOSIM and NAOSIM-FI is overestimated over the entire period in all polynya subsets. This is confirmed by the statistical parameters shown in Table 2a, b. The mean of NAOSIM open-water area is approximately two times higher than the mean of AMSR-E open-water area. Using the *t*-test, the correlations above 0.12 (November–May long-time series) and above 0.27 (April–May short-time series) turn out to be significant at the 95% confidence level. Low correlations are found between NAOSIM/NAOSIM-FI and AMSR-E open-water areas ($r = -0.06$ to 0.29). In a few cases NAOSIM-FI open-water area is even more overestimated than NAOSIM without landfast-ice (e.g., in the WNS at the end of December). The mean values of NAOSIM and NAOSIM-FI open-water area, however, are similar (LAP: NAOSIM open-water area = 6940 km^2, NAOSIM-FI open-water area = 7054 km^2). The differences between NAOSIM and NAOSIM-FI open-water areas are higher in the eastern Laptev Sea (WNS and AL). In WNS the difference of the mean between both open-water areas is 589 km^2 and in T (western Laptev Sea) the difference is only 115 km^2.

Regarding FESOM from November to May, the open-water areas calculated from the model version with coarse spatial resolution and without including landfast-ice (FESOM-CR) is overestimated (Table 2c). For the T polynya (western Laptev Sea), the mean of FESOM-CR open-water area is approximately 10 times higher than the mean of the AMSR-E data. In the eastern Laptev Sea (WNS, AL) the open-water area is about two times higher. The FESOM-CR open water area correlates weakly with AMSR-E open-water area in all subsets. Moderate correlations are only found in the NET polynya ($r = 0.55$).

During the six weeks from the beginning of April to mid-May, FESOM-CR shows moderate (LAP: $r = 0.70$; AL: $r = 0.49$; T: $r = 0.32$) to high (WNS: $r = 0.87$; NET: $r = 0.86$) correlations with AMSR-E.

Regarding the model run with high spatial resolution (FESOM-HR), the correlations with AMSR-E are lower than with FESOM-CR (e.g., FESOM-HR LAP: $r = 0.46$) except in the AL and T polynyas. The FESOM-HR open-water area is underestimated in the eastern Laptev Sea (WNS, AL) and in agreement with AMSR-E data in the western Laptev Sea (T, NET).

In contrast to the simulations without landfast-ice implementation, FESOM-FI open-water area is largely consistent with AMSR-E data. Only during the polynya opening around 8 April (day 99) the FESOM-FI open-water area becomes overestimated in the WNS. The correlation between FESOM-FI and AMSR-E open-water area is moderate: between 0.63 in the LAP polynya and 0.74 in the T polynya (r is significant for the 95% confidence level).

Comparing the open water area of the three FESOM model runs, the correlation increases from FESOM-CR over FESOM-HR to FESOM-FI in AL and T polynya. In all other polynya subsets, results are ambiguous.

Polynya openings, here characterized by an increase of the open-water area, are visible in all data sets, e.g., the polynya events around 27 March (day 87) in the WNS polynya or in late December/early January (days 361–364) in the AL polynya. However, the duration and magnitude of the increased open-water areas are overestimated in NAOSIM and NAOSIM-FI. In the WNS, a polynya opening occurs in the AMSR-E data at the end of December and lasts for a few days. This event is also visible in the NAOSIM and NAOSIM-FI open-water areas but there it lasts for approximately 13 days. The striking event in the WNS in late April/early May (days 118–126) is underrepresented in NAOSIM open-water area. The NAOSIM-FI open-water area reproduces this event better but a bit earlier in time compared with AMSR-E data.

Polynya activity from FESOM-CR and FESOM-HR shows features similar to those of the NAOSIM time series: the duration of the polynya openings is also overestimated and the striking opening at 29 April (day

Citation: *Polar Research* 2011, *30*, 7124, DOI: 10.3402/polar.v30i0.7124

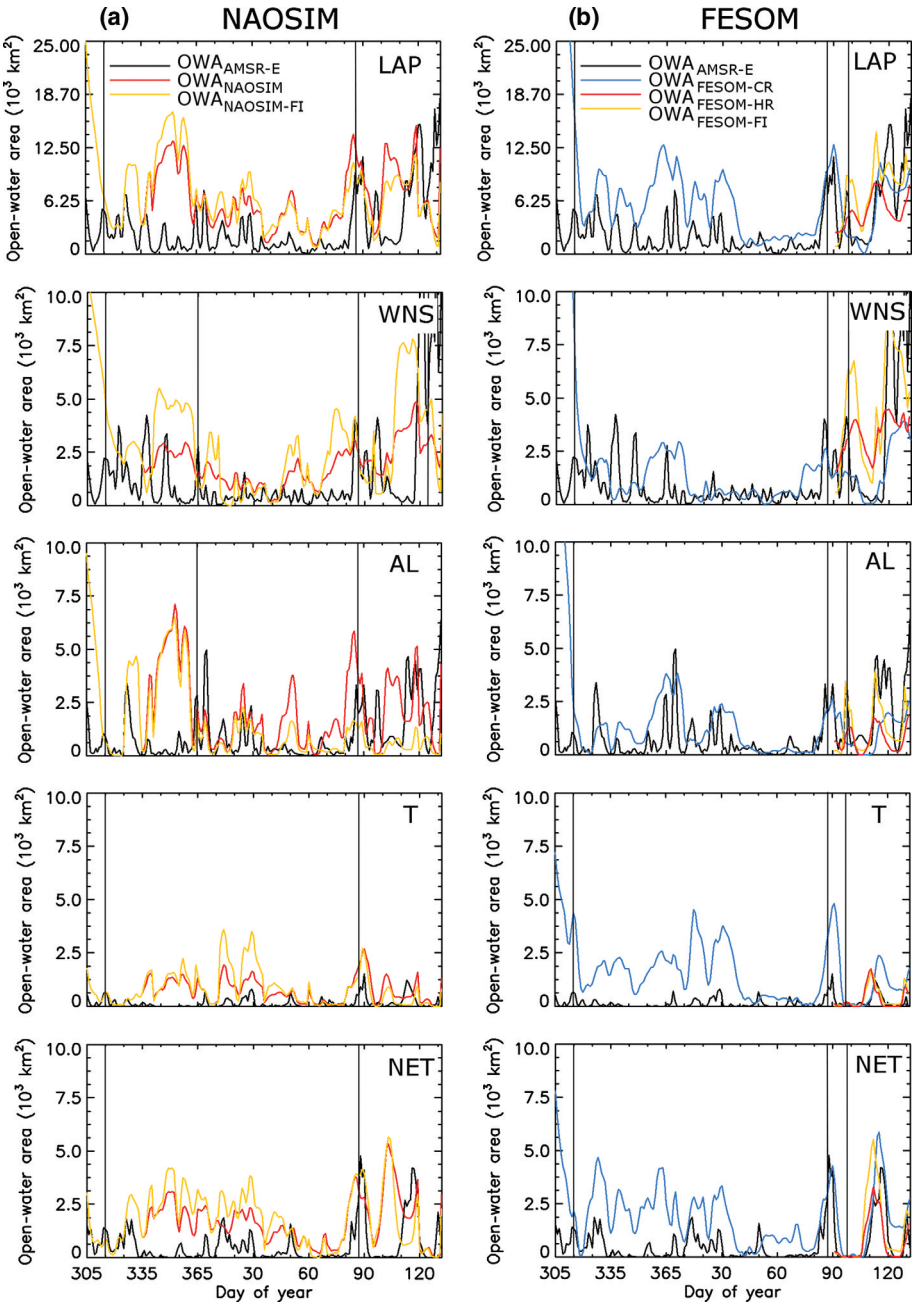

Fig. 3 Time series of open-water areas (OWA) for the whole polynya system (LAP) and the individual Laptev Sea sub-polynyas (see Fig. 2). Open-water areas are calculated from ice concentrations of: (a) the North Atlantic–Arctic Ocean–Sea-Ice Model (OWA_{NAOSIM}) and another version of this model, the NAOSIM-FI ($OWA_{NAOSIM\text{-}FI}$) from 1 November 2007 to 11 May 2008 and (b) the coarse-resolution version of the Finite Element Sea-Ice Ocean Model ($OWA_{FESOM\text{-}CR}$) from 1 November 2007 to 11 May 2008 and two other versions of the FESOM model, FESOM-HR ($OWA_{FESOM\text{-}HR}$) and FESOM-FI ($OWA_{FESOM\text{-}FI}$) from 1 April to 11 May 2008. Open-water areas derived from Advanced Microwave Scanning Radiometer–Earth Observing System (AMSR-E) data ($OWA_{AMSR\text{-}E}$) are shown in (a) and (b). Vertical lines mark polynya events.

120) in the WNS is not well shown. In contrast to this, FESOM-FI open-water area represents this event clearly.

In autumn, from the end of September to mid-November during the freezing over of the Laptev Sea, we find a pronounced overestimation of open-water area in the simulations (see Fig. 3, days 305–319). The NAOSIM and NAOSIM-FI open-water areas are identical during this time, since the formation of landfast ice starts

Table 2 Mean, standard deviation (SD) and correlation coefficients (*r*) of the different open-water area (OWA) time series for all polynya subsets for the period from 1 November 2007 to 11 May 2008 and 1 April to 11 May 2008. Mean and SD of open-water area of (a) the Advanced Microwave Scanning Radiometer-Earth Observing System (AMSR-E), (b) the two versions of the North Atlantic–Arctic Ocean–Sea-Ice Model (NAOSIM and NAOSIM-FI) and (c) the three versions of the Finite Element Sea-Ice Ocean Model (FESOM-CR, FESOM-HR and FESOM-FI). Correlation coefficients between results derived from AMSR-E and NAOSIM/NAOSIM-FI are presented in (b). AMSR-E and FESOM-CR/FESOM-HR/FESOM-FI correlations are presented in (c). Correlations significant at the 95% confidence level (*t*-test) are in boldface.

(a) Remote sensing data set		(b) NAOSIM		(c) FESOM				
Nov–May		Nov–May		Nov–May	Apr–May			
	$OWA_{AMSR\text{-}E}$	OWA_{NAOSIM}	$OWA_{NAOSIM\text{-}FI}$	$OWA_{FESOM\text{-}CR}$	$OWA_{AMSR\text{-}E}$	$OWA_{FESOM\text{-}CR}$	$OWA_{FESOM\text{-}HR}$	$OWA_{FESOM\text{-}FI}$
		Sum of all polynya regions (LAP)						
Mean (km^2)	3105	6940	7054	7205	6651	5471	5058	7552
SD (km^2)	3578	4168	4272	7670	5244	3550	1779	3276
r		**0.14**	0.02	**0.17**		**0.70**	**0.46**	**0.63**
		Western New Siberian polynya (WNS)						
Mean (km^2)	1431	2365	2954	2107	3619	1719	3280	4631
SD (km^2)	2298	1746	2343	3479	3978	1319	862	2580
r		**0.13**	0.06	**0.12**		**0.87**	**0.62**	**0.69**
		Anabar–Lena polynya (AL)						
Mean (km^2)	941	2256	1473	1584	1979	1085	706	1270
SD (km^2)	1248	2004	1916	2345	1727	810	561	1084
r		0.08	−0.06	**0.14**		**0.49**	**0.63**	**0.68**
		Taimyr polynya (T)						
Mean (km^2)	157	691	806	1603	207	978	322	384
SD (km^2)	243	558	828	1391	298	1008	482	478
r		**0.29**	**0.22**	**0.33**		**0.32**	**0.63**	**0.74**
		North-eastern Taimyr polynya (NET)						
Mean (km^2)	576	1628	1821	1911	848	1688	749	1268
SD (km^2)	896	1090	1298	1457	1267	1683	1026	1670
r		**0.22**	**0.13**	**0.55**		**0.86**	**0.81**	**0.71**

in December. In mid-November (around day 319), open-water area calculated from the simulations is on the same level as the satellite values.

Polynya area

Having compared the mean conditions of the modelled sea-ice concentrations in the polynya subsets, we now analyse the development of well-formed polynyas in the simulations. Well-formed polynyas are defined as long narrow areas of open water and thin ice. The polynya area is shown as a time series in Fig. 4 for the WNS and NET polynya. These two polynyas can be regarded as representative of the eastern and western Laptev Sea, respectively. The polynya areas calculated from the two satellite methods (PSSM and sea-ice concentration threshold) are very consistent. The correlation is around 0.99 (Table 3a). Mean values and standard deviations are very similar for both satellite products.

In the eastern Laptev Sea (WNS), the simulated polynya area in NAOSIM is very small over the entire period when compared with AMSR-E and PSSM data (Fig. 4a). Mean and standard deviation of NAOSIM polynya areas are smaller by a factor of two compared with satellite-derived polynya area (Table 3b). In the western Laptev Sea (NET), the NAOSIM polynya area is larger compared with AMSR-E and PSSM from November to February. There is no correlation between NAOSIM and AMSR-E polynya area (WNS: $r = 0.07$; NET: $r = -0.02$) in the two regions of interest.

For NAOSIM-FI (with landfast ice), the polynya size is larger in comparison with NAOSIM. However, in comparison with the observed data sets, the NAOSIM-FI polynya area is overestimated. The date of the openings does not always coincide with satellite-derived polynya area (e.g., polynya events in March). There is also no correlation in comparison with AMSR-E polynya area.

The coarse resolution FESOM simulation shows no polynya after 15 November (day 319) in the WNS polynya (Fig. 4b). Accordingly, there is no correlation between FESOM-CR and AMSR-E polynya area (Table 3c). The mean and standard deviation of the FESOM-CR polynya area in WNS is strongly influenced by the values in the beginning of November. In the

Citation: *Polar Research* 2011, *30*, 7124, DOI: 10.3402/polar.v30i0.7124

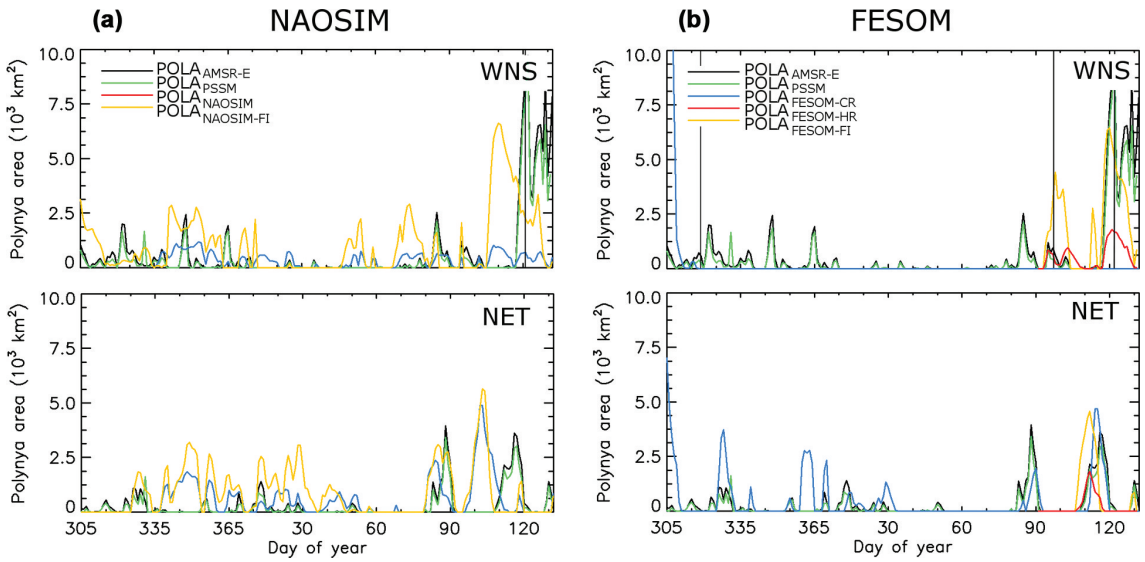

Fig. 4 Time series of polynya areas (POLA) for winter season 2007/08 in the WNS (eastern Laptev Sea) and NET (western Laptev Sea) polynyas (see Fig. 2). Polynya areas are calculated from ice concentrations of (a) the North Atlantic–Arctic Ocean–Sea-Ice Model ($POLA_{NAOSIM}$) and another version of this model, the NAOSIM-FI ($POLA_{NAOSIM\text{-}FI}$) from 1 November 2007 to 11 May 2008 and (b) the coarse-resolution Finite Element Sea-Ice Ocean Model ($POLA_{FESOM\text{-}CR}$) from 1 November 2007 to 11 May 2008 and two other versions of the FESOM model, FESOM-HR ($POLA_{FESOM\text{-}HR}$) and FESOM-FI ($POLA_{FESOM\text{-}FI}$) from 1 April to 11 May 2008. Polynya areas derived from Advanced Microwave Scanning Radiometer–Earth Observing System (AMSR-E) data ($POLA_{AMSR\text{-}E}$) and the Polynya Signature Simulation Method ($POLA_{PSSM}$) are shown in (a) and (b). After day 319 (vertical line) FESOM-CR shows no polynya area. The vertical line at day 99 marks an overestimation of FESOM-FI open-water area. Vertical line at day 121 in WNS marks a polynya event.

western Laptev Sea (NET) polynya activity is better represented by FESOM-CR polynya area. In the first half of the winter the FESOM-CR polynya area is overestimated while in the second half we find good agreement with AMSR-E and PSSM data.

Regarding the period from 1 April to 11 May, no polynya occurs in the eastern Laptev Sea (WNS). In the western Laptev (NET), the correlation between FESOM-CR and AMSR-E is high ($r = 0.79$) and means and standard deviations are similar.

Increasing the spatial resolution and reducing the diffusivity in the FESOM model causes polynya activity in the WNS. However, FESOM-HR polynya area is underestimated in both polynya regions. The correlation is moderate.

The implementation of landfast ice leads to an increase of polynya area in both polynya regions. The FESOM-FI polynya area is roughly consistent with AMSR-E data in both parts of the Laptev Sea ($r = 0.56$–0.60), but mean and standard deviation in the FESOM-FI polynya area show more consistency with AMSR-E polynya area in the NET than in the WNS polynya. In line with the overestimation of the FESOM-FI open-water area, we find an overestimation of the FESOM-FI polynya area in the WNS for the opening in early April (around day 99).

The increased spatial resolution in FESOM-HR yields ambiguous results in terms of polynya simulation. Only when a landfast-ice mask (FESOM-FI) is implemented do the results show clear improvements. Further below we consider why model improvements in FESOM do not always yield better results.

Case study

In the following, we consider the major polynya event that occurred in the eastern Laptev Sea with a duration of several days at the end of April (days 118–126) in more detail. For this event the daily average sea-ice distributions of NAOSIM, NAOSIM-FI, FESOM-CR, FESOM-HR and FESOM-FI at 29 April (day 120) are shown in Figs. 5 and 6 as an example. Regarding NAOSIM and NAOSIM-FI sea-ice concentrations, polynya areas are visible in both maps. However, there is a striking difference between the NAOSIM and NAOSIM-FI sea-ice fields. The polynya in NAOSIM sea-ice concentrations is positioned along the coastline. In NAOSIM-FI sea-ice fields, it is located at the edge of the landfast ice, making these data more consistent with AMSR-E concentrations. Differences are found in polynya shape and size and the NAOSIM-FI sea-ice distribution is very homogeneous in comparison with AMSR-E data, as seen in Fig. 5d.

Table 3 Mean, standard deviation (SD) and correlation coefficients (*r*) of the different polynya area (POLA) time series for the western New Siberian polynya (WNS) and north-eastern Taimyr polynya (NET) for the period from 1 November 2007 to 11 May 2008 and 1 April to 11 May 2008. Mean and SD of polynya area of (a) the Advanced Microwave Scanning Radiometer-Earth Observing System (AMSR-E) and the Polynya Signature Simulation Method (PSSM), (b) the two versions of the North Atlantic–Arctic Ocean–Sea-Ice Model (NAOSIM and NAOSIM-FI) and (c) the three versions of the Finite Element Sea-Ice Ocean Model (FESOM-CR, FESOM-HR and FESOM-FI). Correlation coefficients between results derived from AMSR-E and PSSM are presented in (a). AMSR-E and NAOSIM/NAOSIM-FI correlation are presented in (b). AMSR-E and FESOM-CR/FESOM-HR/FESOM-FI correlation are presented in (c). Correlations significant at the 95% confidence level (*t*-test) are in boldface.

(a) Remote sensing data sets			(b) NAOSIM		(c) FESOM				
Nov–May			Nov–May		Nov–May	Apr–May			
	$POLA_{AMSR-E}$	$POLA_{PSSM}$	$POLA_{NAOSIM}$	$POLA_{NAOSIM-FI}$	$POLA_{FESOM-CR}$	$POLA_{AMSR-E}$	$POLA_{FESOM-CR}$	$POLA_{FESOM-HR}$	$POLA_{FESOM-FI}$
Western New Siberian polynya (WNS)									
Mean (km^2)	1065	806	632	1553	521	3529	0	837	3128
SD (km^2)	2592	2147	689	2135	3628	4722	0	852	3071
r		**0.99**	0.07	0.10	0.00		0.00	**0.59**	**0.60**
North-eastern Taimyr polynya (NET)									
Mean (km^2)	471	364	870	1322	717	958	821	320	1092
SD (km^2)	1028	845	1291	1708	1630	1556	1939	689	2086
r		**0.98**	−0.02	0.10	**0.43**		**0.79**	**0.68**	**0.56**

Clearly, a large number of mainly straight leads are simulated with NAOSIM and NAOSIM-FI. On 29 April, leads are simulated in the north-east and the central part of the Laptev Sea (Fig. 5a, b). Figure 7 shows the relative distribution of the simulated leads from December to May. To identify the leads, we again use the 70% sea-ice concentration threshold. Areas with high frequencies up to 84% denote polynyas. Next to the polynya regions, areas with sea-ice concentrations below 70% occur with frequencies up to 50% farther offshore. The increase of open-water area in these regions results from openings of simulated leads.

In contrast, FESOM-CR simulations without landfast ice yield no WNS polynya area but a very homogeneous ice coverage with some thinning in the eastern Laptev Sea (Fig. 6a). There, the ice concentration reaches 79%. Examination of the FESOM-CR simulations during the winter season shows that well-formed polynyas are not visible over the entire period (see Fig. 4b). Instead, FESOM-CR simulations feature a sea-ice concentration reduced by 60–80% over a larger area in the polynya regions during the events.

The high-resolution model FESOM-HR simulates coastal polynyas with open-water areas along the coastline and increasing ice coverage within the polynya going farther offshore (Fig. 6b).

With landfast ice, FESOM-FI ice concentrations show better results. Distinctive polynyas are simulated (Fig. 6c) and the comparison with AMSR-E sea-ice fields shows a large degree of consistency with the polynya location but also a small shift towards the coastline, as seen in the difference plot (Fig. 6f).

Table 4 summarizes the general findings of the five simulations. The comparison between the results for open-water area (Table 2) and polynya area (Table 3) show a general overestimation of open-water area calculated from modelled sea-ice concentrations, while the polynya area is underestimated for simulations without landfast ice. In FESOM and NAOSIM, the reason for this is that a large open-water area does not correspond to the formation of a well-formed polynya with strongly reduced sea-ice concentration. In fact, the large open-water area in the simulations results from slightly reduced sea-ice concentration over large areas. Regarding the polynya position, polynyas are not present or at the wrong location in runs without landfast ice.

The FESOM-HR is an exception because the polynyas are simulated at the wrong position with a high ice-concentration gradient within the polynyas. In regions (e.g., NET and WNS) where, in reality, the polynyas are located near to the coast of the mainland or an island due

Citation: *Polar Research* 2011, *30*, 7124, DOI: 10.3402/polar.v30i0.7124

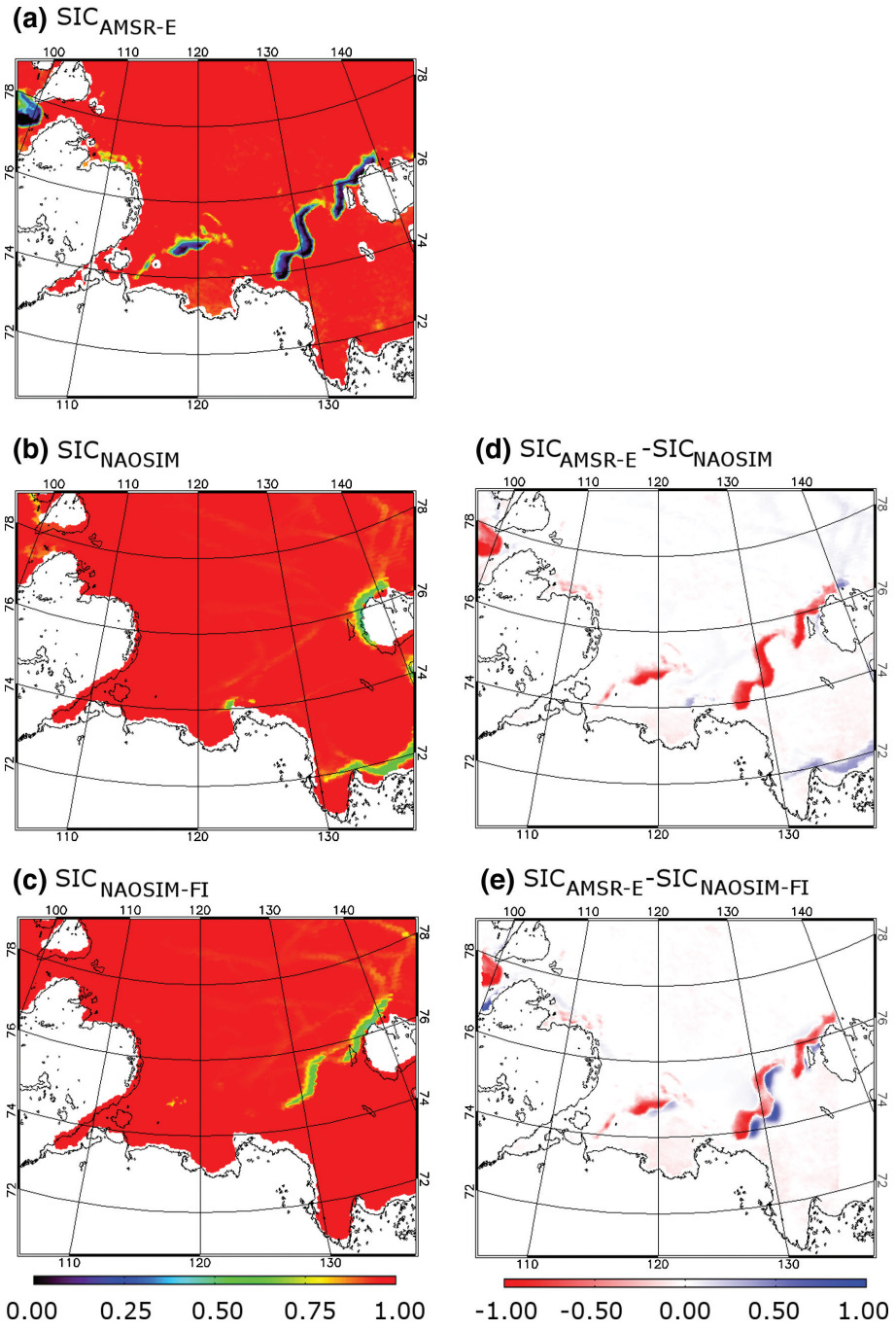

Fig. 5 Maps of sea-ice concentration (SIC) on 29 April 2008 derived from (a) Advanced Microwave Scanning Radiometer–Earth Observing System (AMSR-E) data, (b) the North Atlantic–Arctic Ocean–Sea-Ice Model (NAOSIM) and (c) another version of this model, NAOSIM-FI. In (a) and (b) yellow–green features denote the polynyas, light orange features indicate leads. Plots showing the difference that results when (d) NAOSIM and (e) NAOSIM-FI simulations are subtracted from the AMSR-E sea-ice concentration.

to a small landfast-ice area, the agreement with AMSR-E is better as it is in regions with a large landfast-ice extension (e.g., AL).

For simulations that include landfast ice, the polynyas are simulated at the correct positions. However, examination of the NAOSIM-FI open-water area shows that in some cases the overestimation is higher compared with the NAOSIM open-water areas (Fig. 3a). This results from the still continuing overestimation of the open-water area plus the now realistically located polynya.

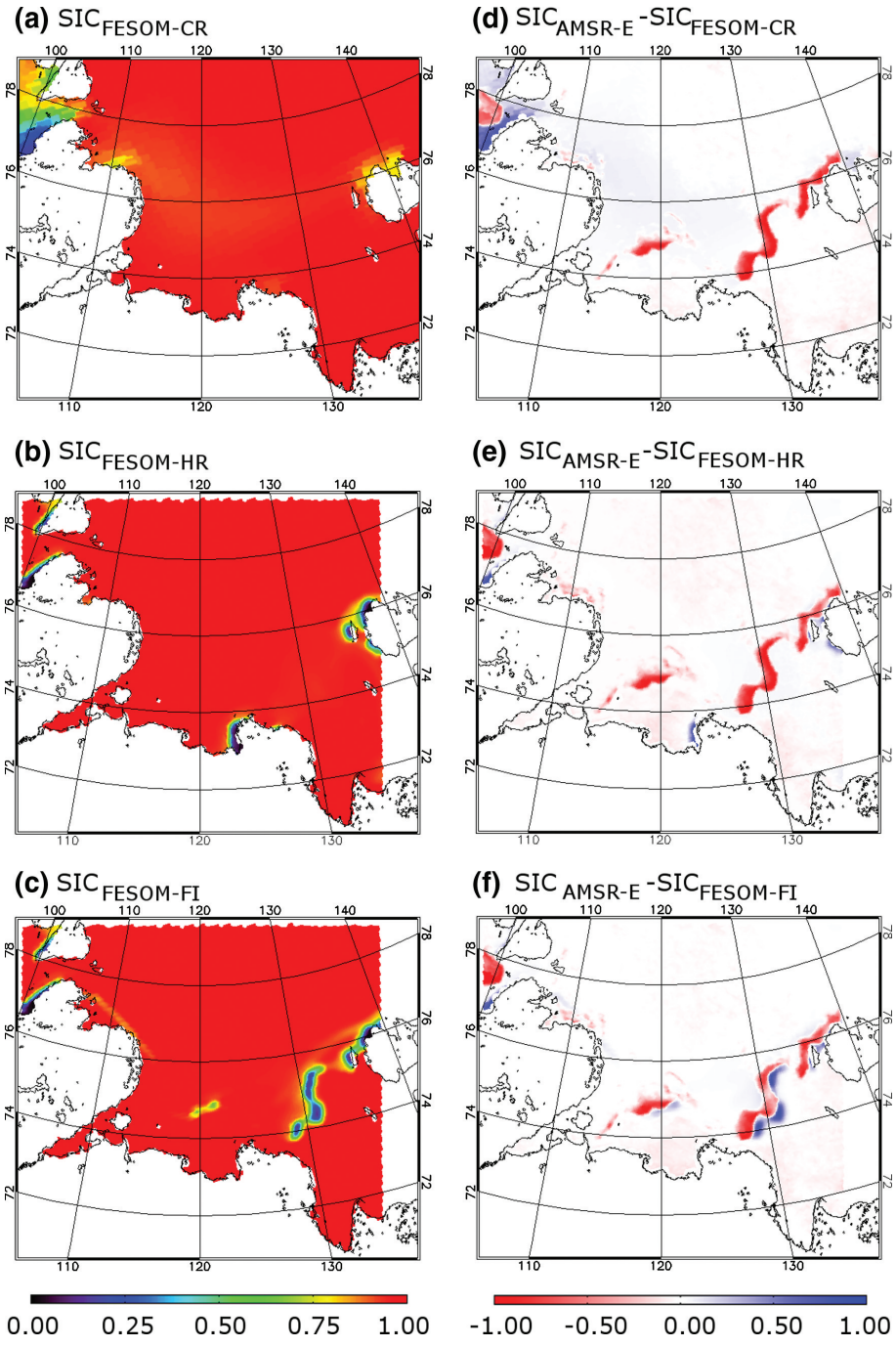

Fig. 6 Maps of sea-ice concentration (SIC) on 29 April 2008 derived from (a) the coarse-resolution Finite Element Sea-Ice Ocean Model (FESOM-CR); and two other versions of this model, (b) FESOM-HR and (c) FESOM-FI. Plots showing the difference that results when (d) FESOM-CR, (e) FESOM-HR and (f) FESOM-FI simulations are subtracted from the AMSR-E sea-ice concentration (compare to Fig. 5a).

Discussion

The intercomparison of polynya areas from satellite data using two different algorithms shows a very strong correlation between the two data sets. Despite the fact that sea-ice concentration errors can be up to 10%, at lower concentrations even higher (Andersen et al. 2007; Spreen et al. 2008) and that the PSSM has a slight tendency to underestimate polynya area (Willmes et al.

Citation: *Polar Research* 2011, *30*, 7124, DOI: 10.3402/polar.v30i0.7124

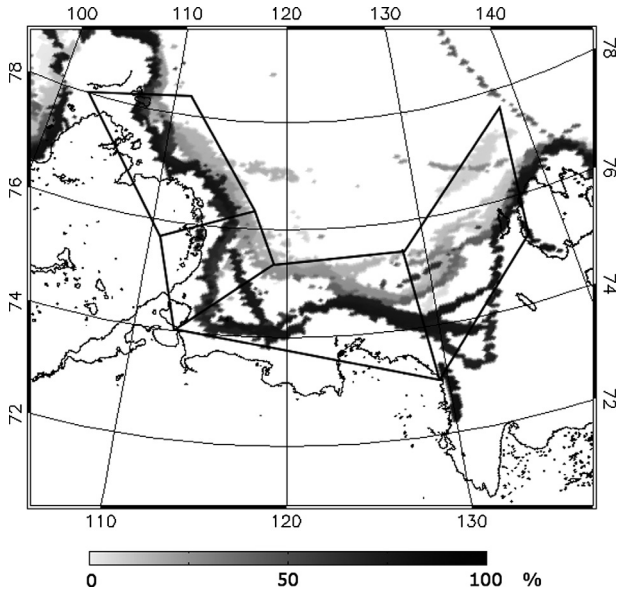

Fig. 7 Sea-ice concentrations derived from the NAOSIM-FI version of the North Atlantic–Arctic Ocean–Sea-Ice Model are examined in terms of the occurrence of leads. The criterion is the 70% sea-ice concentration threshold that is also used for the classification of polynyas and includes open water and thin ice up to 0.2-m thickness (Willmes et al. 2010). Pixels with a sea-ice concentration below 70% are counted from 1 December 2007 to 11 May 2008. The map shows the frequency (%) of these pixels in the period in question. The darker grey areas along the fast-ice edge indicate polynyas. The lighter grey areas indicate simulated leads not attached to the fast-ice edge but located in the defined polynya regions. Black boxes indicate the polynya regions (see Fig. 2).

2010), both data sets appear to give reliable estimates of the true polynya conditions.

A previous comparison of NAOSIM sea-ice concentrations with passive microwave satellite products from Kauker et al. (2003) shows the general agreement of both data sets on a large-scale in terms of the long-term mean state and the interseasonal variability of the simulated sea-ice concentrations. This is supported by Wang et al. (2003), who demonstrated that current sea-ice/ocean models put more emphasis on the representation of large-scale sea-ice extent and concentration in the Arctic and Antarctic. Consequently, the distribution of sea-ice concentration is very smooth with only gentle gradients in the NAOSIM and FESOM simulations that have a coarse spatial resolution and excluded fast-ice. This effect is particularly visible in the FESOM-CR simulations, which are even more coarse-scale than the NAOSIM runs.

While it seems appropriate to match the large-scale sea-ice distribution, it also leads to a blurring of the polynya signature (Wang et al. 2003) so that the simulated sea-ice concentration is too high at the polynya location and too low in the drift-ice and landfast-ice

Table 4 Comparison of sea-ice concentrations (SIC) and polynya features simulated by the five different model runs: two versions of the North Atlantic–Arctic Ocean–Sea-Ice Model (NAOSIM) and three versions of the Finite Element Sea-Ice Ocean Model (FESOM).

Feature	NAOSIM	NAOSIM with landfast ice (NAOSIM-FI)	FESOM without landfast ice, coarse resolution (FESOM-CR)	FESOM without landfast ice, high resolution (FESOM-HR)	FESOM with landfast ice, high resolution (FESOM-FI)
SIC in general	Generally underestimated	Generally underestimated	Generally underestimated	Except for polynya regions: good agreement	Good agreement
Polynya location	Dislocation, located at the coastline	Realistic location at the landfast-ice edge	Dislocation, located at the coastline	Dislocation, located at the coastline	Realistic location at the landfast-ice edge
Polynya shape	Follows the coastline	In general good, small differences	Large areas with slightly reduced SIC, no well-formed polynya	Depends on coastline, no agreement with AMSR-E	Accurate
SIC in polynya	Uniformly distributed, lowest SIC are not reproduced	Uniformly distributed, lowest SIC are not reproduced	No well-formed polynya, slightly reduced SIC over a large area	Small-scale gradients, lowest SIC are reproduced	Small-scale gradients, lowest SIC are reproduced

areas. The spatial smoothing of the sea-ice concentration could also induce a smoothing in time that would explain the overestimated duration of the polynya activity.

There are two basic reasons for the smoothing of sea-ice concentration in space and time. The first is an insufficient spatial resolution in our NAOSIM and FESOM-CR simulations as well as an insufficient spatial and temporal resolution of the forcing data. Due to a grid space of approximately 25 km, this effect is even more crucial in the FESOM-CR version than in NAOSIM (grid space approximately 9 km). This problem also appears in the improved NAOSIM model simulations because the resolution of NAOSIM-FI and the forcing data is not increased. A second reason is that FESOM-CR simulations were run with a relatively large horizontal diffusivity (2000 m^2/s), which clearly produces very smooth ice concentration fields and a deceptive weakening of polynya signatures.

The AMSR-E data show zero or very low sea-ice concentrations at the fast-ice edge; going farther offshore, the sea-ice concentrations increase (Fig. 5a). This graduated distribution is not reproduced by NAOSIM, NAOSIM-FI and FESOM-CR simulations. Rather, the sea-ice concentrations are homogeneously distributed within the polynya at medium concentrations. The minima of ice concentrations are not shown (Figs. 5, 6). This implies that the simulated polynyas consist mostly of thin ice with only little open water. Consequently, the heat fluxes between ocean and atmosphere in both the NAOSIM and the FESOM-CR model runs would be too low. According to Ebner et al. (2011), thin ice of around 5 cm reduces the turbulent exchange of sensible and latent heat by up to 270 W/m^2, dependent on near-surface wind speed and the temperature conditions between thin ice and the atmosphere.

Rollenhagen et al. (2009) point out a general underestimation of ice concentrations (i.e., an overestimation of open-water area) from FESOM in comparison with satellite data. This is consistent with our results of the original FESOM-CR and NAOSIM model runs. In NAOSIM the overestimation of open water is primarily caused by the overestimated number of leads in the entire Laptev Sea in wintertime (see Fig. 7). The narrow elongated shape of the leads may result from the ice rheology that is used (Rozman 2009). Additionally, a coarse horizontal resolution has an impact on the underestimation of the ice concentration. Polynyas are sub-grid scale phenomena for coarse-resolution models. To mimic the effect of polynyas, the model simulates low concentrations in a broader area. Furthermore, the daily wind forcing data (i.e., temporally smoothed wind fields) cannot resolve short-term events that may be crucial for a realistic description of polynya formation.

In NAOSIM-FI the overestimation of open water is even larger due to the coarse resolution of the model, the smoothed forcing data and the spurious leads plus the now realistically located polynya area.

In FESOM-HR (for April and May 2008) the spatial resolution has been increased (now approximately 5-km grid spacing) and the forcing data have a higher spatial resolution (40 km compared with 200 km in NCEP data). Additionally, horizontal diffusion has been reduced (100 m^2/s compared with 2000 m^2/s in FESOM) in order to avoid a spurious smoothing of sea-ice concentrations. The sea-ice concentration simulations of this model show that a fine spatial resolution and a reduced diffusivity alone do not lead to improvements (Figs. 3, 4). As explained above, a coarse spatial resolution and a high diffusivity coefficient result in a smoothing of the sea-ice concentration. Thus, errors of the model in terms of small-scale effects (e.g., polynyas) are masked. In the fine-scale model version these errors emerge stronger. For instance, uncertainties in the momentum fluxes (transfer coefficient and wind forcing) might lead to an overestimation of open water and polynya area, e.g., in the WNS polynya around 8 April (day 99). Improvements of the turbulence closure scheme, e.g., stability-dependent transfer coefficients, are of rising importance when resolution is increased. However, the gradual increase of ice concentrations within the polynya showing very low concentrations at the coast to levels of approximately 70% farther seawards in the polynya is well reproduced.

Concluding the analysis of the model versions without fast-ice prescription in terms of polynyas (small-scale features), we see that the models are able to reduce the sea-ice concentrations during polynya events but they mostly overestimate the fraction of open water in the polynya regions (Fig. 3). Regarding the sea-ice fields (Figs. 5, 6), the reason for the reduction of ice concentrations becomes clear. As mentioned above, the smoothing of the ice concentration and the coarse spatial resolution are important for this effect, not the simulation of realistic polynyas (Fig. 4). When polynyas are simulated they are not located in the expected regions. As well, the improved model run FESOM-HR is not able to resolve this problem. At this point, it becomes obvious that landfast ice has to be included. Sea-ice models are currently not able to simulate the formation of landfast ice (see above). This implies that modifications in the numerics of the model (with our current knowledge) would not lead to improvements concerning the location of the polynyas. Hence, a kind of fast-ice parameterization is essential for

Citation: *Polar Research* 2011, *30*, 7124, DOI: 10.3402/polar.v30i0.7124

a realistic simulation of the small-scale processes in the Laptev Sea.

The improvement of the model results with implementation of landfast ice can be clearly seen in the sea-ice fields of both models (Figs. 5d, 6f). The NAOSIM-FI and FESOM-FI sea-ice concentrations show correctly simulated polynyas along the edge of landfast ice. The small displacement of the polynya between AMSR-E and NAOSIM-FI/FESOM-FI data could result from the difference between the two remote-sensing data sets. For the fast-ice edge, we used the high resolved MODIS data (1-km spatial resolution) and for the comparison we used the daily available but more coarsely resolved AMSR-E data (6.25-km spatial resolution).

The introduction of landfast ice has a more pronounced effect in the eastern part of the Laptev Sea due to the greater extent of landfast ice in this region. In the western part of the Laptev Sea, along the Taimyr Peninsula, the extent of the landfast ice is only 10 to 20 km due to the very steep slope of the seafloor reported by Reimnitz et al. (1995). In particular, FESOM-CR open-water area is seriously overestimated in the western Laptev Sea in comparison with the eastern Laptev Sea. This means that in FESOM (the same is valid for NAOSIM) the polynyas are also correctly positioned in the western Laptev Sea when no landfast ice is involved.

Besides the realistic location of the polynya, the graduated sea-ice distribution within the polynya, which is simulated by FESOM-HR, is retained in FESOM-FI.

In future studies, other parameterizations and numerics should be adapted to allow a better representation of local, small-scale processes. The NAOSIM needs to be improved with respect to horizontal resolution of the model grid and the forcing data. Regarding the FESOM-FI, the use of high-resolution wind fields in space and time together with an optimized scheme for advection and diffusion is expected to further improve the simulation of local sea-ice conditions. Further NAOSIM developments will include a higher temporal resolution of the wind fields, for example, from daily to six-hourly resolution, with the aim of improving the simulation of ice concentrations.

As mentioned above, the turbulence closure scheme and momentum fluxes could be optimized in FESOM and NAOSIM to minimize the errors that appear due to fine resolution.

Summary and conclusions

In this study we evaluate simulated sea-ice concentrations from five different model simulations in the Laptev Sea for the 2007/08 winter season, focusing on the improvement that results from implementing a landfast-ice mask. As reference data sets, we use sea-ice concentrations derived from AMSR-E brightness temperatures and the polynya areas classified by PSSM using passive microwave data. We compare open-water and polynya areas and analyse sea-ice distribution fields of a selected polynya event. Our results agree with the findings of Wang et al. (2003) and Rollenhagen et al. (2009), namely, that simulated sea-ice concentrations are underestimated and spuriously smoothed. While model fields generally represent accurately the large-scale sea-ice conditions in the Arctic, major differences are found for the Laptev Sea polynyas. However, the results of those model runs that include a prescribed landfast-ice mask indicate that the main goal—the simulation of realistically located polynyas—is achieved by both models. Taking into account the incapability of the current sea-ice/ocean models to simulate the formation of landfast ice, the necessity of a prescribed landfast-ice mask is essential. Without a fast-ice implementation, other model modifications are not able to raise sufficiently the quality of the simulations on smaller scales (see FESOM-HR simulations). However, it becomes also clear that model improvements in terms of a realistic sea-ice concentration simulation are more complex and the implementation of a landfast-ice mask alone is not sufficient.

Adaptions to smaller scales have been applied to FESOM. Besides a correctly located polynya, the mean sea-ice concentrations are well simulated in the FESOM-FI fine-scale version with increased spatial resolution, reduced horizontal diffusivity, prescribed fast-ice mask and high-resolution forcing data. Therefore, we suggest the following improvements for NAOSIM on a regional scale: (1) increasing the spatial resolution of the model, (2) using finer spatially and temporally resolved forcing data and (3) optimizing the diffusion and advection scheme. For NAOSIM and FESOM on a regional scale we propose: (1) improving the turbulence closure scheme (e.g., the stability-dependent transfer coefficient) and (2) optimizing momentum fluxes (transfer coefficient and wind forcing). In terms of landfast ice, the optimum solution would be the reproduction of landfast ice by the model itself as part of its own dynamics. We conclude that further improvements of all model components—parameterizations as well as numerics—have to be reconsidered if the model simulations in polynya regions are to be further improved.

Acknowledgements

AMSR-E ASI are provided by the University of Hamburg. AMSR-E brightness temperatures are acquired from the

National Snow and Ice Data Center. MODIS brightness temperatures are provided by the US National Aeronautical and Space Administration Level 1 and Atmosphere Archive and Distribution System. Support from Dr Sven Harig during the installation of the FESOM model on the University of Trier's computing server is gratefully acknowledged. This study is funded by the German Ministry for Education and Research Laptev Sea System project (grant no. 0360639E).

References

Andersen S., Tonboe R., Kaleschke L., Heygster G. & Pedersen L.T. 2007. Intercomparison of passive microwave sea ice concentration retrievals over the high-concentration Arctic sea ice. *Journal of Geophysical Research—Oceans 112*, C08004, doi: 10.1029/2006/JC003543.

Barber D.G. & Hanesiak J.M. 2004. Meteorological forcing of sea ice concentrations in the southern Beaufort Sea over the period 1979 to 2000. *Journal of Physical Oceanography 109*, C06014, doi: 10.1029/2003JC002027.

Bareiss J. 2003. *Freshwater input and fast ice in the East Siberian Arctic—results from surface and satellite observations as well as sensitivity studies using a thermodynamic fast-ice model. Reports on Polar and Marine Research 442*. Bremerhaven: Alfred Wegener Institute for Polar and Marine Research.

Bareiss J. & Görgen K. 2005. Spatial and temporal variability of sea ice in the Laptev Sea: analyses and review of satellite passive-microwave data and model results, 1979 to 2002. *Global and Planetary Change 48*, 28–54.

Cavalieri D., Markus T. & Comiso J. 2004. *AMSR-E/Aqua Daily L3 12.5 km brightness temperature, sea ice concentration, & snow depth polar grids V002, November 2007–May 2008*. Digital media. Updated daily. Boulder, CO: National Snow and Ice Data Center.

Dethleff D., Loewe P. & Kleine E. 1998. The Laptev Sea flaw lead—detailed investigations on ice formation and export during 1991/1992 winter season. *Cold Regions Science and Technology 27*, 225–243.

Ebner L., Schröder D. & Heinemann G. 2011. Impact of the Laptev Sea flaw polynyas on the atmospheric boundary layer and ice production using idealized mesoscale simulations. *Polar Research 30*, xx(-art no-)xx, doi: xxxxxxxx (this volume).

Fieg K., Gerdes R., Fahrbach E., Beszczynska-Möller A. & Schauer U. 2010. Simulation of oceanic volume transports through Fram Strait 1995–2004. *Geophysical Research Letters 60*, 491–450.

Gerdes R., Karcher M.J., Kauker F. & Schauer U. 2003. Causes and development of repeated Arctic Ocean warming events. *Geophysical Research Letters 30*, article no. 1980, doi: 10.1029/2003GL018080.

Hibler W.D. 1979. A dynamic thermodynamic sea ice model. *Journal of Physical Oceanography 88*, 2873–2887.

Hibler W.D. & Bryan K. 1987. A diagnostic ice–ocean model. *Journal of Physical Oceanography 17*, 987–1015.

Hunke E.C. & Dukowicz J.K. 1997. An elastic–viscous–plastic model for sea ice dynamics. *Journal of Physical Oceanography 27*, 1849–1868.

Johnson M., Gaffigan S., Hunke E. & Gerdes R. 2007. A comparison of Arctic Ocean sea ice concentration among the coordinated AOMIP model experiments. *Journal of Geophysical Research—Oceans 112*, C04S11, doi: 10.1029/2006JC003690.

Kaleschke L., Lüpkes C., Vihma T., Haarpaintner J., Bochert A., Hartmann J. & Heygster G. 2001. SSM/I sea ice remote sensing for mesoscale ocean–atmosphere interaction analysis. *Canadian Journal of Remote Sensing 27*, 526–537.

Kanamitsu M., Ebisuzaki W., Woollen J., Yang S.-K., Hnilo J.J., Fiorino M. & Potter G.L. 2002. NCEP-DOE AMIP-II reanalysis (R-2). *Bulletin of the Atmospheric and Meteorological Society 83*, 1631–1643.

Karcher M.J., Gerdes R., Kauker F. & Köberle C. 2003. Arctic warming: evolution and spreading of the 1990s warm event in the Nordic seas and the Arctic Ocean. *Journal of Geophysical Research—Oceans 108*, article no. 3034, doi: 10.1029/2001JC001265.

Kauker F., Gerdes R., Karcher M.J., Köberle C. & Lieser J. 2003. Variability of Arctic and North Atlantic sea ice: a combined analysis of model results and observations from 1978 to 2001. *Journal of Geophysical Research—Oceans 108*, article no. 3182, doi: 10.1029/2002JC001573.

Kern S. 2008. Polynya area in the Kara Sea, Arctic, obtained with microwave radiometry for 1979–2003. *Geoscience and Remote Sensing Letters 5*, 171–175.

Kern S. 2009. Wintertime Antarctic coastal polynya area: 1992–2008. *Geophysical Research Letters 36*, L14501, doi: 10.1029/2009/GL038062.

Kern S., Spreen G., Kaleschke L., De la Rosa S. & Heygster G. 2007. Polynya Signature Simulation Method polynya area in comparison to AMSR-E 89 GHz sea-ice concentrations in the Ross Sea and off Adelie Coast, Antarctica, for 2002–2005: first results. *Annals of Glaciology 46*, 409–418.

Key J.R., Collins J.B., Fowler C. & Stone R.S. 1997. High-latitude surface temperature estimates from thermal satellite data. *Remote Sensing of Environment 61*, 302–309.

König Beatty C. 2007. *Arctic landfast sea ice*. PhD thesis, Department of Mathematics, New York University.

König Beatty C. & Holland D.M. 2009. Modeling landfast sea ice by adding tensile strength. *Journal of Physical Oceanography 40*, 185–198.

Lieser J.L. 2004. *A numerical model for short-term sea ice forecasting in the Arctic. Reports on Polar and Marine Research 485*. PhD thesis, University of Bremen.

Lietaer O., Fichefet T. & Legat V. 2008. The effects of resolving the Canadian Arctic Archipelago in a finite element sea ice model. *Ocean Modelling 24*, 140–152.

Mahoney A., Eicken H., Gaylord A.G. & Shapiro L. 2007. Alaska landfast sea ice: links with bathymetry and atmospheric circulation. *Journal of Geophysical Research—Oceans 112*, C02001, doi: 10.1029/2006JC003559.

Citation: *Polar Research* 2011, *30*, 7124, DOI: 10.3402/polar.v30i0.7124

Majewski D., Liermann D., Prohl P., Ritter B., Buchhold M., Hanisch T., Paul G., Wergen W. & Baumgardner J. 2002. The operational global icosahedral-hexagonal grid point model GME: description and high resolution tests. *Monthly Weather Review 130*, 319–388.

Markus T. & Burns B.A. 1995. A method to estimate subpixel-scale coastal polynyas with satellite passive microwave data. *Journal of Geophysical Research—Oceans 100*, 4473–4487.

Martin T. & Gerdes R. 2007. Sea ice drift variability in Arctic Ocean Model Intercomparison Project models and observations. *Journal of Geophysical Research—Oceans 112*, C04S10, doi: 10.1029/2006JC003617.

Massom R.A., Harris P.T., Michael K.J. & Potter M.J. 1998. The distribution and formative processes of latent-heat polynyas in East Antarctica. *Annals of Glaciology 27*, 420–426.

Morales Maqueda M.A., Willmott A.J. & Biggs N.R.T. 2004. Polynya dynamics: a review of observations and modeling. *Reviews of Geophysics 42*, RG1004, doi: 10.1029/2002RG000116.

Pacanowski R.C. 1995. *MOM 2 documentation, user's guide and reference manual. GFDL Ocean Group Technical Report 3*. Princeton, NJ: Geophysical Fluid Dynamics Laboratory, Princeton University.

Parkinson C.L. & Washington W.M. 1979. A large-scale numerical model of sea ice. *Journal of Geophysical Research—Oceans 84*, 311–337.

Reimnitz E., Eicken H. & Martin T. 1995. Multiyear fast ice along the Taymyr Peninsula, Siberia. *Arctic 48*, 359–377.

Renfrew I.A., King J.C. & Markus T. 2002. Coastal polynyas in the southern Weddell Sea: variability of the surface energy budget. *Journal of Geophysical Research—Oceans 107*, article no. 3063, doi: 10.10.1029/2000JC000720.

Rollenhagen K., Timmermann R., Janjic T., Schröter J. & Danilov S. 2009. Assimilation of sea ice motion in a finite-element sea ice model. *Journal of Geophysical Research—Oceans 114*, C05007, doi: 10.1029/2008JC005067.

Rozman P. 2009. *The role of the Laptev Sea fast ice in an Arctic Ocean–sea ice coupled model*. Master's thesis, Alfred Wegener Institute for Polar and Marine Research.

Spreen G., Kaleschke L. & Heygster G. 2008. Sea ice remote sensing using AMSR-E 89 GHz channels. *Journal of Geophysical Research—Oceans 113*, C02S03, doi: 10.1029/2005JC003384.

Timmermann R., Danilov S., Schröter J., Böning C., Sidorenko D. & Rollenhagen K. 2009. Ocean circulation and sea ice distribution in a finite element global sea ice–ocean model. *Ocean Modelling 27*, 114–129.

Wang J., Kwok R., Saucier F.J., Hutchings J., Ikeda M., Hibler W. III, Haapala J., Coon M.D., Meier H.E.M., Eiken H., Tanaka N., Prentki D. & Johnson W. 2003. Working toward improved sea ice–ocean modeling in the Arctic seas. *Eos, Transactions of the American Geophyscial Union 84*, 325–336.

Willmes S., Adams S., Schroeder D. & Heinemann G. 2011. Spatiotemporal variability of sea-ice coverage, polynya dynamics and ice production in the Laptev Sea between 1979 and 2008. *Polar Research 30*, article no. 5971, doi: 10.3402/polar.v30i0.5971 (this volume).

Willmes S., Krumpen T., Adams S., Rabenstein L., Haas C., Hoelemann J., Hendricks S. & Heinemann G. 2010. Cross-validation of polynya monitoring methods from multi-sensor satellite and airborne data: a case study. *Canadian Journal of Remote Sensing 36*, 196–210.